Cambridge Centre for Computational Chemical Engineering

University of Cambridge

Department of Chemical Engineering

Preprint ISSN 1473 – 4273

A detailed model for the sintering of polydispersed nanoparticle agglomerates

Markus Sander [1] , Richard H. West [1] , Matthew S. Celnik [1] and Markus Kraft [1]

released: 16 February 2009

[1] Department of Chemical Engineering and Biotechnology
University of Cambridge
New Museums Site
Pembroke Street
Cambridge, CB2 3RA
UK
E-mail: mk306@cam.ac.uk

Preprint No. 67

c4e

Key words and phrases: SiO2, modelling, sinter, stochastic, particle

Edited by
Cambridge Centre for Computational Chemical Engineering
Department of Chemical Engineering
University of Cambridge
Cambridge CB2 3RA
United Kingdom.

Fax: + 44 (0)1223 334796
E-Mail: c4e@cheng.cam.ac.uk
World Wide Web: http://www.cheng.cam.ac.uk/c4e/

Abstract

In this study the coagulation, condensation and sintering of nanoparticles is investigated using a stochastic particle model. Each stochastic particle consists of interacting polydisperse primary particles which are connected to each other. In the model sintering occurs between each individual pair of neighboring primary particles. This is important for particles in which the range of the size of the primary particles varies significantly. The sintering time is obtained form the viscous flow model. The model is solved using a stochastic particle algorithm. The particles are represented in a binary tree which contains the connectivity as well as the degree of sintering information. Particles are formed, coagulate, sinter and experience condensation according to known rate laws. The particle binary tree, along with it the degree of sintering, is updated after each time step according to the rates of the different processes. The stochastic particle method uses the technique of fictitious jumps and linear process deferrment. The theoretical results are validated against experimental values for the formation of SiO_2 nanoparticles and computer generated TEM pictures are presented and compared to experiments.

Contents

1 Introduction

The formation of nanoparticles from gaseous precursors is becoming more and more important in the production of new materials. Inception, coagulation, condensation and sintering are the important steps to form these particles. The inception of a particle is induced by a collision of two precursors from the gas-phase. These first particles grow due to condensation of molecules from the surrounding gas-phase or further collisions with other particles. Condensation leads to an increase of particle volume and also increases the sphericity. Sintering reduces the surface of the particles and makes them rounder whereas the coagulation of particles decreases the sphericity of the particles. The relative timescale of the sintering and the coagulation processes determines the shape and the size of the particles. The faster the sintering is, the rounder the particles become.
Koch and Friedlander [8] have developed a model explaining particle growth by coagulation and sintering. They have generalized the Smoluchowski equation to incorporate the coalescence rate into a model for aerosol dynamics. Xiong and Pratsinins [29] have established a two-dimensional sectional model to describe the evolution of the particle size and shape of particles. Seto et al. [22, 23] have studied the sintering of SiO_2 and TiO_2 particles in a heated pipe and determined the structure and size distribution. They have also used a two-dimensional sectional model to represent the size distribution and to solve the population balance equation. Their model explains the growth of primary particles and the shrinkage of the particles due to sintering and they concluded that the temperatures at which sintering occurs are 50-100% of the bulk melting points. This work has been extended in a later study by Nakaso et al. [12]. The computational performance of different population balance models has been investigated by Mühlenweg et al [11].
Some researchers have found that the liquidity of the primary particles depends strongly on the size of the primary particles [17, 26, 27]. The melting point decreases with the size of the primaries, therefore Rogak [17] introduced a critical primary size D_{melt}. He assumes that the primaries are liquid like below D_{melt} and therefore they coalesce instantly. Rogak also concluded that the primary particle diameter is much less sensitive to temperature than would be expected from simple sintering models. Tsantilis and Pratsinis [26] have developed a simple sectional model describing the evolution of primary and aggregate size distributions. Their model has been applied to aerosol synthesis of TiO_2 by $TiCl_4$ oxidation in a hot wall reactor. They also stated that sintering is quite slow for large primary particles compared to small primaries. In a further study Tsantilis et al. [27] have introduced a critical primary particle diameter $d_{p,min}$ in the mathematical expression for the characteristic sintering time to take the change of fluidity of small primaries into account.
In most of these studies a equal sized primary particles are assumed, however Venkateshwarlu and Helble [30] investigated the coalescence of unequal-sized amorphous primary particles. Their results indicate that the normalized sintering rate is independent of the size ratio of the two interacting primary particles and that the smaller primary particle determines primarily the sintering rate. Heine and Pratsinis [7] have developed a two dimensional sectional population balance model that relates the rate of sintering to each individual primary particle size. Schmid et al. [20, 21] have presented a three-dimensional model for aggregates undergoing sintering and coagulation where the particles are modeled as overlapping spheres. They concluded that the fractal dimension depends strongly

on the concurrent coagulation and sintering process.
Akhtar et al. [1] have developed a Monte Carlo simulation on a 2-D lattice to describe the coagulation and sintering of nanoclusters. Sintering has been implemented in their model using a random particle walk on the surface of the cluster. They have also investigated the fractal dimension of the particles and concluded that the surface area of the particles is more sensible to changes in the sintering rate than the fractal dimension.

In our work a stochastic method is used to solve the population balance equation and the sintering is calculated individually for each pair of neighbouring primary particles. Stochastic techniques do not suffer from the numerical diffusion inherent in sectional methods and are able to provide the full multivariate particle population density without additional constraints. Various algorithms have been developed to reduce the computational time required for the solution of the population balance equation [14]. Stochastic particle models have already been used to investigate the particle size distribution of soot [3, 10, 16, 18, 24, 25]. Morgan et al [9] have used a stochastic particle model to simulate coagulation, condensation, and sintering, however in contrast to our work the sintering is calculated as an average for the entire particle.
The processes described by the current model are: coagulation, condensation and sintering. The simulation in this work models the particle formation process starting from the first sticking of two molecules from the gas-phase. The model maintains a list of particles where each particle contains a data structure that stores the primary particles. This data structure also contains the level of sintering between touching primary particles. The coagulation of paricles is implemented using the free collision kernel. Sintering, which is driven by the excess surface area of the particle compared to a spherical particle with the the same volume [8, 29], is not calculated as an average for the entire particle, but is implemented for each pair of neighboring primaries individually. This is important if the sintering time depends on the size of the primary particles as reported in [17, 26, 27]. The primary particles are not equal-sized and change their size due to sintering and condensation processes. The current sintering model is included in the stochastic population balance solver developed by Celnik et al. [2].
In the next section the different processes implemented in the model are described in more detail. Afterwards the mathematical implementation and the data structure is presented. Finally the model is validated against experiments using data for the formation of SiO_2 nanoparticles in a hot wall reactor from Seto et al. [23]. Agglomerates are generated at 900°C and the change of the shape of the particles due to sintering is evaluated by heating the particles to different final temperatures. The primary particle diameter distribution and the average primary particle diameter is evaluated and computer generated TEM style images are created to compare the model with experimental data.

2 Particle Structure Model

2.1 General Description and Reaction Rates

In the current work the system is represented by a stochastic particle ensemble. These particles interact according to the rates for the different processes: sintering, condensation, coagulation and inception. The number of stochastic particles is limited by the maximum number of particles N_{max}, which determines the accuracy of the simulation. Eibeck and Wagner [4, 5] have demonstrated for a time-independent univariate system undergoing coagulation and fragmentation that the system converges to the solution of the model if $N \rightarrow \infty$. Each particle contains a data structure where the primary particles are stored that belong to the particle. The data structure stores also the connections between the primaries and the sintering level between each pair of touching primaries. The rates for

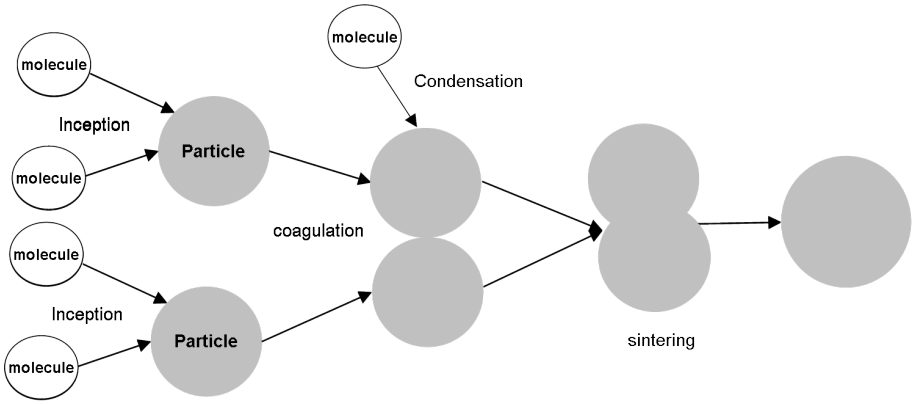

Figure 1: *Different steps in the formation of nanoparticles*

the processes (Figure 1) included in the current model are:

1. Inception: A new particle is inserted in the particle ensemble each time two molecules from the gas-phase collide. The rate is calculated using the transition kernel [15] which is the harmonic mean of the slip-flow and free molecular kernels.

$$R_{inception} = \frac{1}{2} k_{tr} {N_A}^2 C^2 \tag{1}$$

   where k_{tr} is the transition regime coagulation kernel constant, N_A is Avodgadro's number, C is the gas-phase concentration of the incepting species.

2. Coagulation: The coagulation rate R_{coag} of two particles P_i and P_j is proportional to the free molecular collision kernel:

$$K^{fm}(i,j) \propto \left(\frac{1}{m(i)} + \frac{1}{m(j)} \right)^{\frac{1}{2}} (d_c(i) + d_c(j))^2 \tag{2}$$

   where m is the mass and d_c the collision diameter.

3. Condensation: A molecule from the gas-phase which collides with a particle sticks on the particle and increases the mass of the particle. This process is implemented in the model assuming that the collision of a molecule from the gas-phase and a particle can be calculated using the free molecular collision kernel for the particle and a single molecule from the gas phase. The rate takes the form

$$R_{cond} = 2.2\eta C \sqrt{\frac{\pi k_B T}{2m}} (d + d_c)^2 \tag{3}$$

where C, m and d are the gas-phase concentration, mass and collision diameter of the condensing species respectively. d_p is the collision diameter of the particle, η the efficiency of the collision.

4. Sintering: The sintering rate R_{sinter} depends mainly on the excess surface of the particle over a spherical particle with the same mass. A particle reduces the free surface to minimize the free energy. This results in the rounding of the particle, finally to a sphere. The asymptotic equation

$$\frac{da}{dt} \propto -\frac{1}{\tau}(a - a_{final}) \tag{4}$$

describing the sintering of a particle with the surface a, a spherical surface a_{final} (the surface of a sphere with the same volume as the particle) and a characteristic sintering time τ, developed by Frenkel [6], has been used to calculate the sintering. The sintering has been calculated by solving equation 4 individually for each pair of neighboring primary particles. More details about the implementation of sintering will be given in the next section.

This model extends the previous two-dimensional surface-volume model [13] and the primary particle list model [28]. The surface-volume model tracks the volume and the surface area of each particle as independent variables. The primary particle list model extends the surface-volume model by adding a list of primary particles for each particle. This primary particle list allows the generation of TEM like pictures, however the actual structure of the particle is not stored in these models and the extend of sintering is calculated by solving equation 4 as an average for the entire particle. This is an issue especially when the characteristic sintering time depends on the size of each primary particle as reported in previous studies [17, 26, 27] and the primaries have a broad size distribution.

2.2 State Space

In this model it is assumed that each particle

$$P_i = P_i(p_1, ..., p_n, \mathbf{C}, \mathbf{I}, \mathbf{S}) \tag{5}$$

consists of n primary particles p. The index $i = 1, ..., N$, where N is the number of particles in the system. n and N vary in time. Each primary

$$p_j = p_j(v_j) \tag{6}$$

has a volume v_j. The matrices $\mathbf{C}$, $\mathbf{I}$ and $\mathbf{S}$ describe the sintering between the primary particles:

1. $[\mathbf{C}]_{i,j}$ stores the common surface of primary p_i and p_j. This value is changed due to sintering.
2. $[\mathbf{I}]_{i,j}$ provides the sum of the surfaces of primary p_i and p_j before they start to sinter.
3. $[\mathbf{S}]_{i,j}$ contains the surface of a sphere with the same volume than primary p_i and p_j.

The matrices are quadratic and the dimension is the number of primaries belonging to the particle. The entries i, j of the three matrices are 0 if the primaries p_i and p_j are not touching.

$$[\mathbf{C}]_{i,j} = [\mathbf{S}]_{i,j} = [\mathbf{I}]_{i,j} = 0 \tag{7}$$

if p_i is not a neighbor of p_j. The sintering level $s(i, j)$ between two primaries p_i and p_j is defined using these matrices:

$$s(i,j) = \frac{\frac{[\mathbf{S}]_{i,j}}{[\mathbf{C}]_{i,j}} - \frac{[\mathbf{S}]_{i,j}}{[\mathbf{I}]_{i,j}}}{1 - \frac{[\mathbf{S}]_{i,j}}{[\mathbf{I}]_{i,j}}} \tag{8}$$

The sintering level $s(i, j)$ is 0 if the two primary particles have just collided and is 1 if the two primary particles are fully sintered. $s(i, j)$ is set to 0 the particles p_i and p_j are not neighboring ($[\mathbf{C}]_{i,j} = 0$). The sum of the volumes of all the primaries is equal to the volume V of the particle:

$$V = \sum_{i=1}^{n} v_i. \tag{9}$$

The surface of the particle is approximated by the sum of the surface of all the primary particles assuming that the primaries are spherical:

$$A = \sum_{i=1}^{n} \pi^{\frac{1}{3}} (6v_i)^{\frac{2}{3}}. \tag{10}$$

2.3 Jump Processes

The mathematical implementation of the inception, coagulation, condensation and sintering processes are presented in this section.

2.3.1 Inception

The collision of two molecules in the gas phase is treated as a particle coagulation event and a spherical particle consisting of one primary containing the volume of the two molecules is inserted into the particle ensemble. An inception event increases the number of particles N by 1.

$$\text{molecule} + \text{molecule} \rightarrow P_{N+1}(p_1, \mathbf{C}, \mathbf{I}, \mathbf{S}) \tag{11}$$

The matrices $\mathbf{C}$, $\mathbf{I}$ and $\mathbf{S}$ have the dimension 1×1 and the only entry is 0. The primary particle p_1 has the volume of the two molecules.

2.3.2 Coagulation

The coagulation of particle P_i and particle P_j is implemented as follows in the model:

$$P_i + P_j \rightarrow P_k(p_1, ..., p_{n(P_i)}, p_{(n(P_i)+1)}, ..., p_{n(P_k)}, \mathbf{C}, \mathbf{I}, \mathbf{S}) \tag{12}$$

where $n(P_i)$ is the number of primaries belonging to particle P_i and $n(P_k) = n(P_i) + n(P_j)$ the number of primaries belonging to particle P_k. The primary particles of the new particle P_k are the primary particles of the particle P_i and particle P_j. Therefore the number of primary particles l is equal to the number of primaries of particle P_i plus the number of primaries of particle P_j. The matrix $\mathbf{C}(P_k)$ has the dimension $l \times l$ and is calculated as:

$$\mathbf{C}(P_k) = \begin{pmatrix} & \vdots & \\ \cdots & \mathbf{C}(P_i) & \cdots & [C]_{b,a} & \cdots \\ & \vdots & & \vdots & \\ \cdots & [C]_{a,b} & \cdots & \mathbf{C}(P_j) & \\ & \vdots & & & \end{pmatrix} \tag{13}$$

where $\mathbf{C}(P_k)$ is the matrix $\mathbf{C}$ belonging to particle P_k. A primary p_a from particle P_i and a primary particle p_b from particle P_j are selected randomly. It is assumed that these two primaries are the point where the two particles stick together. The matrices $\mathbf{C}$, $\mathbf{I}$ and $\mathbf{S}$ are changed to include the sintering of these two primaries in the model. $[C]_{a,b} = [C]_{b,a}$ and $[I]_{a,b} = [I]_{b,a}$ is set to the sum of the surface of primary p_a and p_b. $[S]_{a,b} = [S]_{b,a}$ is set to the surface of a sphere with the same volume than primary p_a and p_b. The matrices $\mathbf{I}$ and $\mathbf{S}$ are calculated in the same way. After the creation of particle P_k the two particles P_i and P_j are removed from the system.
The free molecular collision kernel (equation 2) is used to calculate the collision rate between two particles. The collision diameter d_c of a particle P_i is calculated as

$$d_c = \frac{6V}{A} n^{\left(\frac{1}{1.8}\right)} \tag{14}$$

where the fractal dimension d_f is assumed to be 1.8 [19]. The Linear Process Deferment Algorithm (LPDA) [14] has been used to improve the computational performance.

2.3.3 Condensation

In a condensation process a molecule from the gas phase attaches to a particle P_j. The rate for this process is calculated using the free molecular collision kernel for a collision between the molecule from the gas-phase and the particle (equation 3). This is modeled by increasing the volume of a randomly selected primary p_i of particle P_j by the volume of a the colliding molecule. It is assumed that the sintering rate is not affected by a condensation process.

$$p_i(v_i) \rightarrow p_i(v_i + v_s) \tag{15}$$

where v_s is the volume of the colliding molecule. The change in sphericity due to condensation processes is not yet considered in this model because the main aim of this work is to investigate the sintering of particles due to the reheating of the particles.

2.3.4 Sintering

The sintering process is modeled assuming that the excess agglomerate surface area over that of a spherical particle with the same mass decays exponentially [6, 8, 29]. The model described in these studies, which originally describes the average sintering of the entire particle has been modified to describe the sintering between two neighboring primaries p_i and p_j. The matrix $\mathbf{C}$, that contains the common surface of the neighboring primaries is changed as follows:

$$\frac{d[\mathbf{C}]_{i,j}}{dt} = -\frac{1}{\tau}\left([\mathbf{C}]_{i,j} - [\mathbf{S}]_{i,j}\right) \tag{16}$$

The difference between the model used in this work and the most other models is that the sintering is not calculated for the entire particle, but for the individual neighboring primaries. Equation 16 is solved for each pair of neighboring primaries (each non zero entry of matrix $\mathbf{C}$). The characteristic sintering time τ is calculated using the formula introduced in [27]:

$$\tau = A \times d_{i,j} \times \exp\left(\frac{E}{T}\left(1 - \frac{d_{p,min}}{d_{i,j}}\right)\right) \tag{17}$$

where $d_{i,j}$ is the minimum diameter of the two neighboring primaries p_i and p_j. $d_{p,min}$ is the critical diameter below which the primaries are assumed to be liquid like, where the characteristic sintering time is very short. The parameters A, E and $d_{p,min}$ depend on the material and are free parameters in the model. It is assumed that the smallest of the two neighboring primaries determines the sintering time [30]. The diameter of the primaries $d_{i,j}$ used to calculate the characteristic sintering time τ is calculated as:

$$d_{i,j} = 2\left(\frac{3 \times \min(v_i^s, v_j^s)}{4\pi}\right)^{\frac{1}{3}} \tag{18}$$

where

$$v_i^s = v_i + \sum_k s(k,i) \times v_k. \tag{19}$$

k goes over all the neighbors of the primary p_i except primary p_j. The sum over all the neighboring primaries takes the mass transfer due to sintering between neighboring primaries into account, because the volume v_i of primary p_i is only updated when the sintering between two primaries is completed.

It is assumed that two primaries p_i and p_j are completely sintered if the sintering level $s(i,j)$ is greater than 0.95. This is included in the model by replacing primary p_i and p_j by a new primary p_k. The volume of the new primary p_k is the sum of the volumes of the primaries p_i and p_j and the neighboring primaries of the new primary p_k are the neighbors of the primaries p_i and p_j. The quadratic matrix $\mathbf{C}$ is changed by adding a column and a row increasing the dimension from n to $k = n + 1$.

$$\mathbf{C} = \begin{pmatrix} 0 & \cdots & [\mathbf{C}]_{1n} & [\mathbf{C}]_{1k} \\ \vdots & \ddots & \vdots & \vdots \\ [\mathbf{C}]_{n1} & \cdots & 0 & [\mathbf{C}]_{nk} \\ [\mathbf{C}]_{k1} & \cdots & [\mathbf{C}]_{kn} & 0 \end{pmatrix} \tag{20}$$

$$[\mathbf{C}]_{l,k} = [\mathbf{C}]_{k,l} = [\mathbf{C}]_{i,l} + [\mathbf{C}]_{j,l} \tag{21}$$

for $l = 1..k$. Note that it is not possible that $[\mathbf{C}]_{i,l}$ and $[\mathbf{C}]_{j,l}$ are non zero for the same index l. The columns and rows i and j are removed from the matrix. Consequently the dimension of the quadratic matrix $\mathbf{C}$ is reduced by 2. The matrices $\mathbf{I}$ and $\mathbf{S}$ are updated in the same way. Overall the sintering process reduces the dimension of the matrices $\mathbf{C}$, $\mathbf{I}$ and $\mathbf{S}$ by 1 because the number of primaries is reduced due to the sintering event by 1.
In the following we illustrate this using a simple example. The sintering process of a particle consisting of three primaries p_1, p_2 and p_3 is illustrated in Figure 2. Assuming that the three primaries just collided and have not yet sintered (Figure 2(a)), the matrices $\mathbf{C}$, $\mathbf{I}$ and $\mathbf{S}$ are:

$$\mathbf{C} = \begin{pmatrix} 0 & 0 & 0 \\ a & 0 & 0 \\ 0 & b & 0 \end{pmatrix} \mathbf{I} = \begin{pmatrix} 0 & 0 & 0 \\ a & 0 & 0 \\ 0 & b & 0 \end{pmatrix} \mathbf{S} = \begin{pmatrix} 0 & 0 & 0 \\ c & 0 & 0 \\ 0 & d & 0 \end{pmatrix} \tag{22}$$

where a is the sum of the surface of primary p_1 and p_2, b the sum of the surface of primary p_2 and p_3, c and d the surfaces of spheres with the same mass as primaries p_1 and p_2 and primaries p_2 and p_3, respectively. In each time step Δt the evolution of the matrix $\mathbf{C}$ is calculated by integrating equation 16 for all non zero elements of matrix $\mathbf{C}$. The entries of the matrices $\mathbf{I}$ and $\mathbf{S}$ do not change in time, but the dimension changes due to a sintering of coagulation event. After each time step the sintering level s is calculated for each non zero entry in the matrix $\mathbf{C}$ using formula 8. Two primaries are replaced by one primary if the sintering level is higher than the threshold of 0.95. Assuming that primary p_1 and p_2 have reached this threshold at time t_1, primary p_1 and p_2 are replaced by a new primary (Figure 2(c)). The numbering of the primaries is rearranged and the new primary is called p_1. The former primary p_3 is now p_2. The matrices are changed as follows:

$$\mathbf{C} = \begin{pmatrix} 0 & 0 \\ b(t_2) & 0 \end{pmatrix} \mathbf{I} = \begin{pmatrix} 0 & 0 \\ b & 0 \end{pmatrix} \mathbf{S} = \begin{pmatrix} 0 & 0 \\ d & 0 \end{pmatrix} \tag{23}$$

The new primary p_1 has the same volume than the former primaries p_1 and p_2 before the sintering event. The primaries p_1 and p_2 continue to sinter until one spherical primary remains (Figure 2(d)).

3 Data Structure

The data structure and the implementation of the different jump processes in the sintering model is described in this section. In order to ensure a fast selection of the primary particles a binary tree data structure is used. A sample binary tree with the corresponding particle is presented in Figure 3. Each leaf node of the binary tree represents a primary particle. The non leaf nodes do not represent a particle, but they represent a connection between two primary particles. These non leaf nodes of the tree contain the following information:

1. A pointer to the left child (solid lines in Figure 3).

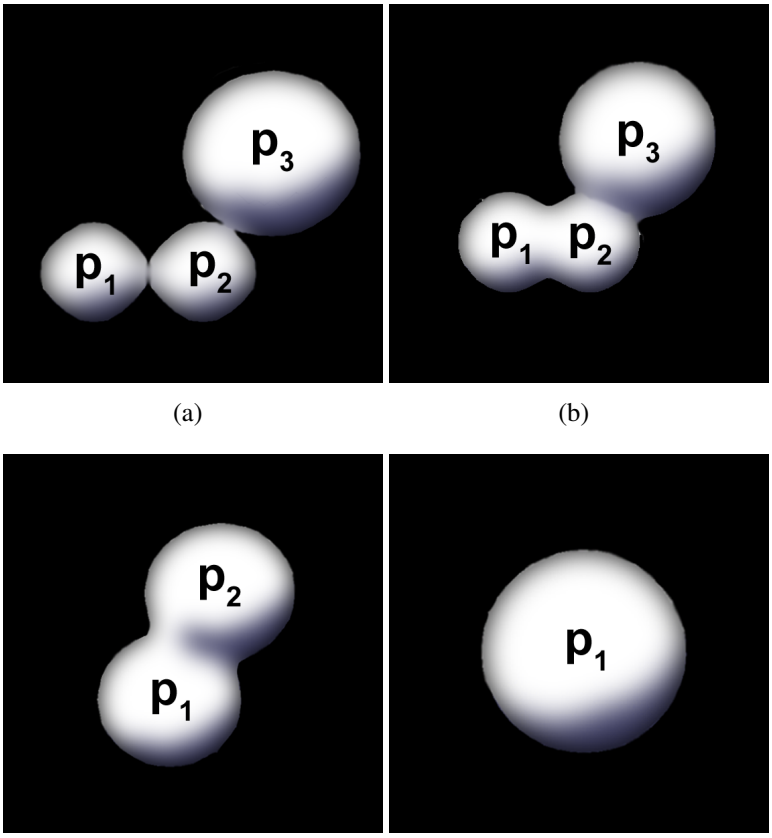

Figure 2: *Evolution of a particle consisting of three primary particles due to sintering. Figure 2(a) shows the particle assuming the primaries p_1, p_2 and p_3 just collided. The primaries are just touching. The primaries have started to sinter in Figure 2(b). After some time primary p_1 and p_2 are completely sintered and replaced by a new primary with the same mass than p_1 and p_2 (Figure 2(c)). The numbering of the primaries is updated. The particle is completely sintered in Figure 2(d)*

2. A pointer to the right child (solid lines in Figure 3).
3. A pointer to a primary belonging to the left subtree, p_i (dashed lines in Figure 3).
4. A pointer to a primary belonging to the right subtree, p_j (dashed lines in Figure 3).
5. The common surface of the primaries p_i and p_j. This entry corresponds to the matrix element $[\mathbf{C}]_{i,j}$.
6. The surface of the primaries p_i and p_j before they start to sinter. This entry corresponds to the matrix element $[\mathbf{S}]_{i,j}$.
7. The surface of a sphere with the same volume than the primaries p_i and p_j. This entry corresponds to the matrix element $[\mathbf{I}]_{i,j}$.

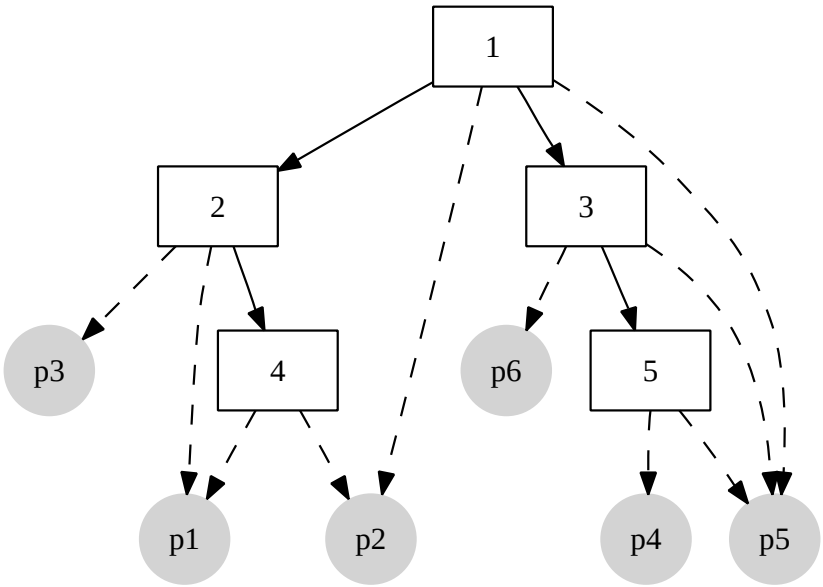

(a) Binary tree

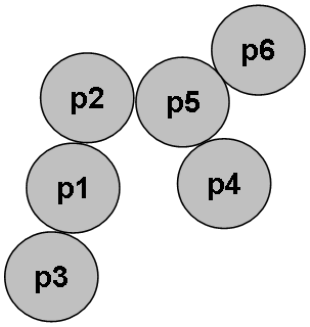

(b) Corresponding particle

Figure 3: *A sample graph for a particle that contains 6 primary particles: p_1,...,p_6. The dashed lines represent the connections between the primary particles.*

8. The sintering level $s(p_i, p_j)$ between the primaries p_i and p_j. This value is calculated using equation 8.
9. The volume that is transferred due to sintering from particle p_i to p_j.
10. The volume that is transferred due to sintering from particle p_j to p_i.

The pointers to the left and right children (enumeration point 1 and 2) and to the left and right primaries (enumeration point 3 and 4) are the same if the child is a leaf. For example see the pointers from node 5 in Figure 3. Each non leaf node points to exactly two primary particles (pointers mentioned in enumeration point 3 and 4). These two primary particles are touching and therefore sintering. The dashed lines in Figure 3 represent these pointers. The sintering matrices $\mathbf{C}$, $\mathbf{I}$ and $\mathbf{S}$ are stored in the non leaf nodes. The solid lines represent the pointers necessary to build the binary tree. The leaf nodes of the three, that represent the primary particles have only one date entry:

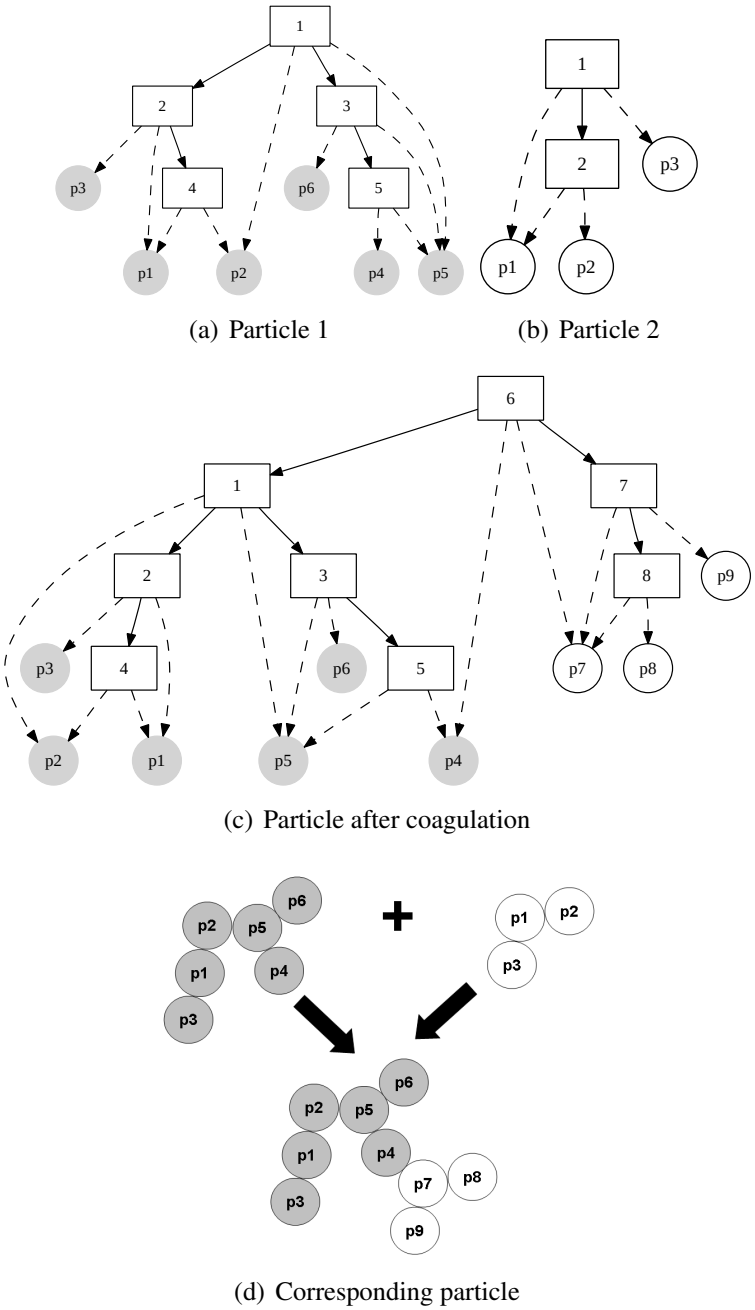

(a) Particle 1 (b) Particle 2

(c) Particle after coagulation

(d) Corresponding particle

Figure 4: *Coagulation of two particles. The two binary trees of particle 1 and 2 are merged together by creating a new root node and adding the two former binary trees as the two children of the root node. Afterwards a primary particle from both particles is selected randomly and a pointer from the root node to these primaries is created. This is the contact point of the two particles. In this example the two primaries are p_4 of the particle 1 and p_1 of the particle 2. Note that in the merged tree the former primary particles of particle 2 are renamed.*

1. The volume of the primary particle.

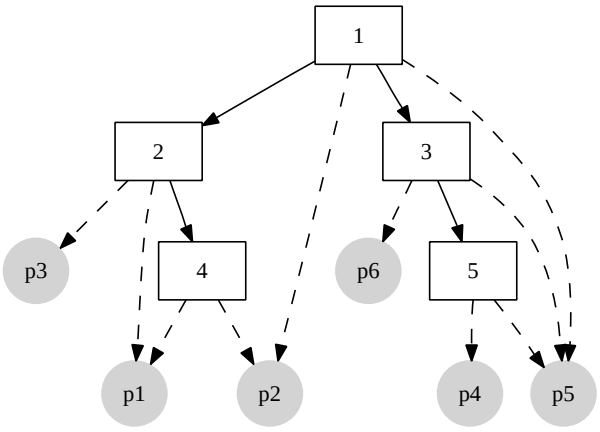

(a) Binary tree before sinter.

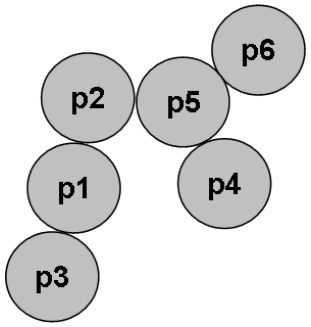

(b) Corresponding particle before sinter

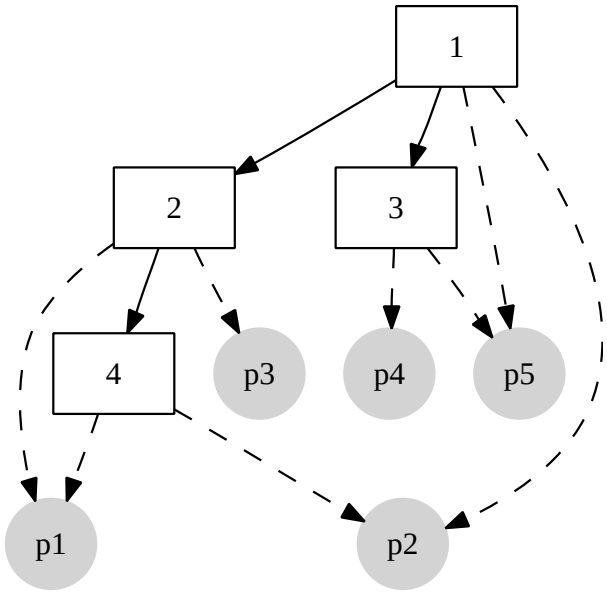

(c) Binary tree after sinter

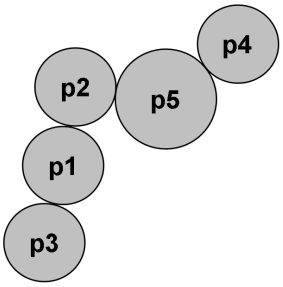

(d) Corresponding particle after sinter

Figure 5: *Sintering of two primary particles (p_4 and p_5) belonging to the same parent node. The primaries are remove from the tree and the parent node is replaced by a new primary particle with the same mass than the two former primaries. Note that the numbering of the primaries is changed after the sintering event.*

3.1 Implementation of Sintering and Coagulation

The coagulation of two particles P_a and P_b is implemented by combining the two individual binary trees. A new root node is created where the left and right subtrees are the trees of the particle P_a respectively P_b. Afterwards two primary particles, p_i and p_j, of particles P_a and P_b respectively are selected randomly and two pointers (the pointers in enumeration point 3 and 4) from the root node to these primaries are set. These two

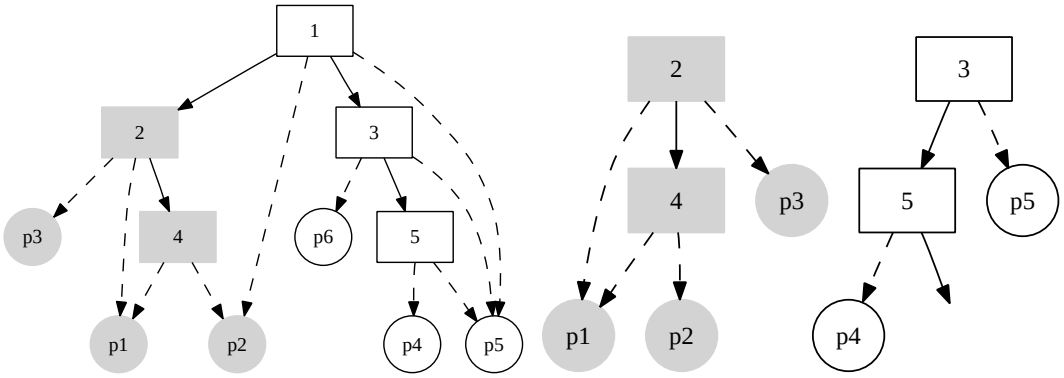

(a) Binary tree before sinter.

(b) Primary particle p_2 has now the volume of the former primary p_2 and the volume of the former primary p_5. The numbering is changed and the former primary p_6 is now primary p_5. The node 1 which connected p_2 and p_5 is removed.

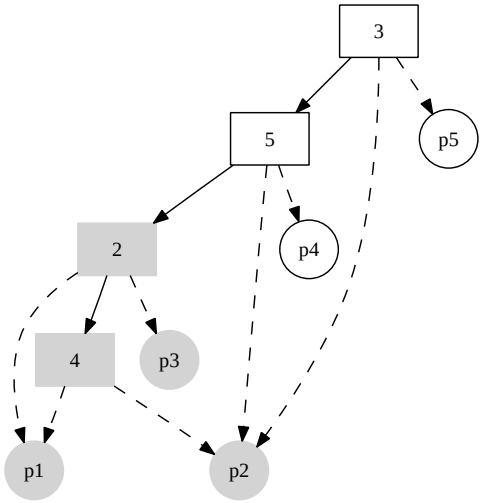

(c) The left subtree of the node 1 is appended at the place where primary p_5 was before the sintering event

Figure 6: *Sintering process if the two primary particles do not belong to the same parent node. It is assumed that the primary particles p_2 and p_5 are completely sintered. The corresponding particle can be seen in Figure 7*

primaries are the contact point of the two particles. The different data entries of the new root node are initialized accordingly.

The sintering of two primary particles is implemented by replacing the two primary particles by one with the same volume. The implementation distinguishes between two cases:

1. The two primary particles belong to the same parent node:
   In this case the two primary particles are removed from the system and the common

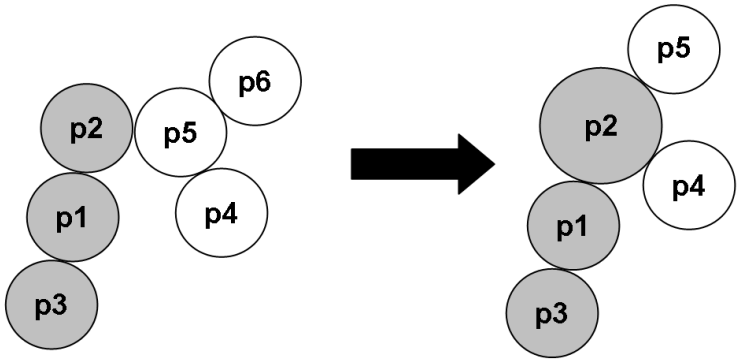

Figure 7: *Corresponding particle to the sintering process shown in Figure 6*

parent node is replaced by a primary particle with the same mass as the two former primary particles. The dashed pointers that pointed to the two former primary particles point now to the new primary. Figure 5 demonstrates the changes in the tree assuming that primary p_1 and primary p_2 are completely sintered.

2. The two primary particles belong to the different parent nodes:
   One of the two primary particles is removed from the system and the second primary particle is replaced by a primary particle with the same volume as the former two primary particles. The node of the tree which pointed (dashed pointer) to the two primary particles is removed and the subtree that contains the primary particle with the mass of the two sintered primaries is appended to the parent node of the first removed primary particle. The dashed pointers that pointed to the two former primary particles point now to the new primary. Figure 6 demonstrates the changes in the tree assuming that primary p_2 and primary p_5 are completely sintered.

3.2 Algorithm

The implementation of the algorithm involves the following steps:

1. Set start time $t \leftarrow t_0$ and the initial system $x \leftarrow x_0$
2. Calculate an exponentially distributed waiting time

$$dt = -\frac{\ln(U)}{R_{tot}} \tag{24}$$

where U is a uniformly distributed random number, $U \in (0, 1)$, and R_{tot} is the total rate of all processes (condensation, coagulation and inception) R_i, $i \in \{coag, inception, cond\}$ defined in section 2.1

$$R_{tot} = \sum_{i=1}^{N} R_i(x, t) \tag{25}$$

3. Increment time variable $t \leftarrow t + dt$.

4. If $t > t_{stop}$ then end.

5. Update the sintering level by integrating equation 16 for the time dt for all the particles.

6. Choose a process i according to the probability:

$$P_i = \frac{R_i}{R_{tot}} \tag{26}$$

7. Perform process.

8. Goto step 2.

4 Validation of the model

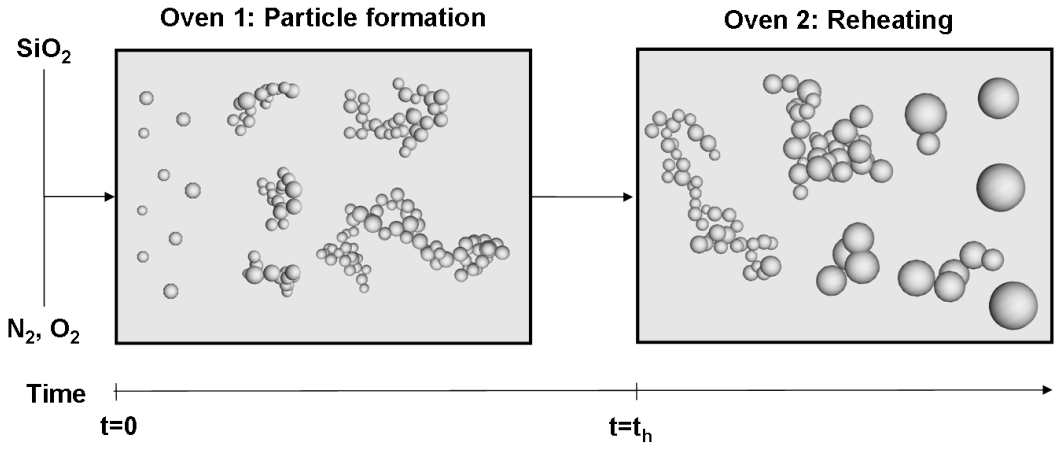

Figure 8: *Different steps in the simulation: The particles grow due to coagulation and condensation at 900°C. The temperature is increased at t=t_h to the final temperature T_f in 0.1s. At the final temperature the particles shrink and the sphericity increases due to sintering.*

The model has been validated against experimental results from Seto et al [23]. The simulation consists of three consecutive steps:

1. The particles are formed at 900°C starting from a gas mixture of SiO_2, O_2 and N_2 for the time t_h.

2. After the creation time t_h the particles are reheated within 0.1s to different final temperatures.

3. The particles remain at the final temperature T_f.

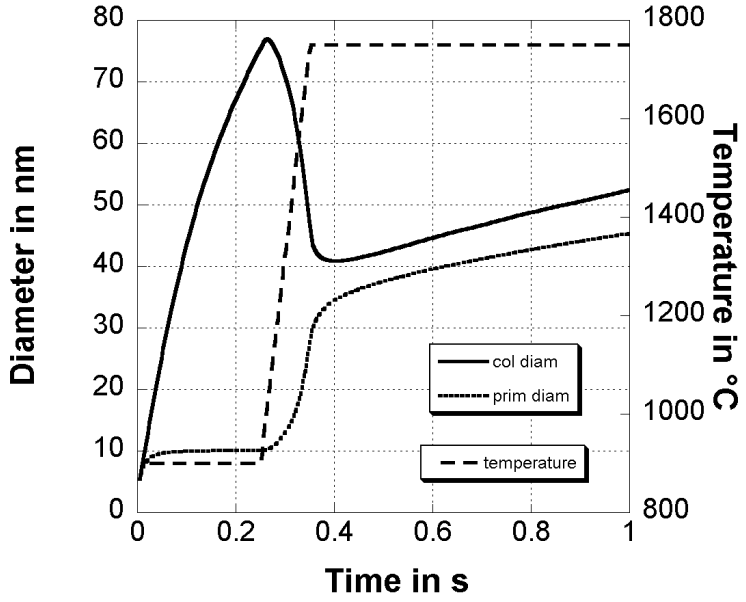

Figure 9: *Evolution of the primary diameter and collision diameter for a final temperature of 1750°C*

Table 1: *Parameters*

Parameter	Value
Collision diameter of SiO_2	0.32 nm
Density of SiO_2	2.2 g/cm^3
Mass of SiO_2	60.084 g/mol
A	6.5×10^{-15}
E	10.2×10^4 K
$d_{p,min}$	3.5×10^{-9} m
Pressure	1 bar
Maximum number of stochastic particles	16384

The time t_h was set to 0.25s in the following simulations if not stated different. The timescale on the graphs represents the entire simulation time. The simulation starts with a mixture of SiO_2, nitrogen and oxygen at 900°C. Chemical reactions in the gas-phase are not included due to the lack of reaction rates and thermochemistry. The pressure was set to 1 bar during the entire simulation. In the beginning of the particle formation each time two silica molecules collide a particle consisting of one primary with the mass of two silica molecules is created. The collision of a particles with a SiO_2 molecule increases the mass of the particle by the mass of a SiO_2 molecule. The SiO_2 molecules are quickly completely converted to particles.
The material dependant sintering parameters A, E and $d_{p,min}$ shown in Table 1 have been determined by fitting the model to the experiments of Seto et al [23]. The determined values are in the same order as those reported in a study from Tsantilis et al. [27].
Figure 9 shows the average primary particle diameter, the collision diameter and the temperature profile for a simulation where the temperature has been increases at t_h=0.25s

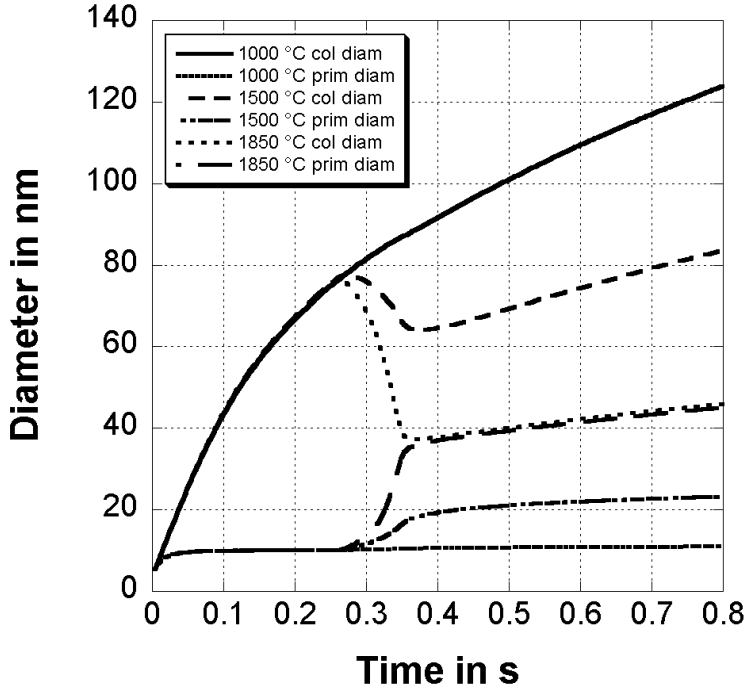

Figure 10: *Comparison of the evolution of the primary diameter and collision diameter for different final temperatures.*

from 900°C to 1750°C within 0.1s. In the beginning the particles remain spherical and consist of only one primary particle because the primaries are quite small and therefore the average sintering time is much shorter than the average time between two collision events. The sintering time increases due to the growth of primaries and when the average primary diameter reaches about 7nm, the particles become non-spherical (the particles consist of more than one primary). This stage is reached after 0.008s. The average primary diameter of the particles grows due to sintering and condensation processes up to 10nm. At this stage the sintering time is much higher than the average time between two collision events. Therefore further collision events result in the formation of agglomerates consisting of many primary particles and sintering is negligible. The average primary diameter remains constant whereas the collision diameter increases. The temperature is increased after 0.25s to 1750°C within 0.1s. The temperature increase reduces the characteristic sintering time and the primary particles sinter together. The average primary diameter increases to 36nm and the collision diameter decreases to 40nm shortly after the temperature increase. The particles reach their final shape very quickly after the temperature increase. The primary particle and collision diameter size distribution follows the step function of the temperature instantaneously, however the collision diameter and the primary diameter still increase slightly due to further collisions between the particles and sintering between the primaries after the temperature increase. The collision diameter is close to the average primary diameter because the particles reach a nearly spherical shape and are composed of only a small number of primary particles.
Figure 10 presents the evolution of the average primary and collision diameter for different final temperatures. The temperature has again been increased after 0.25s from 900°C

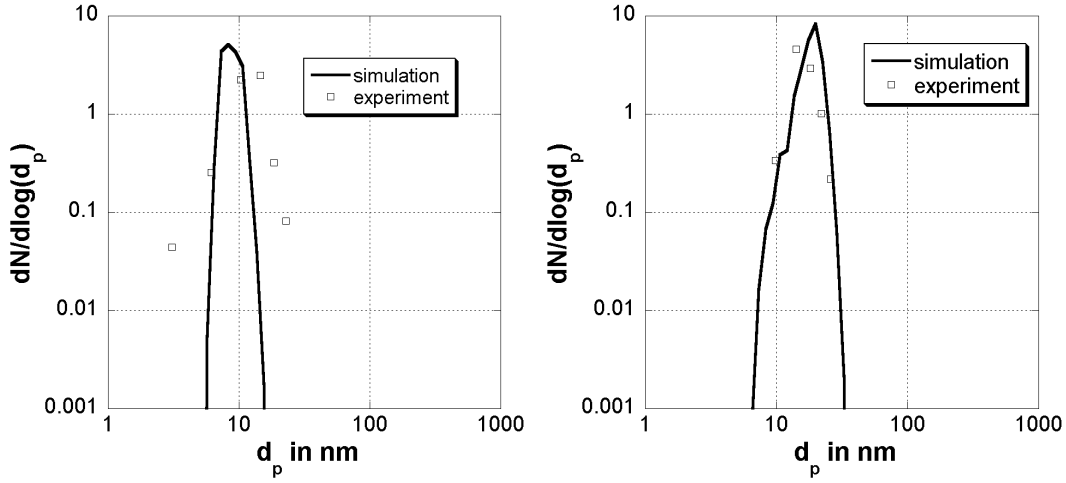

(a) before heating

(b) 1500°C

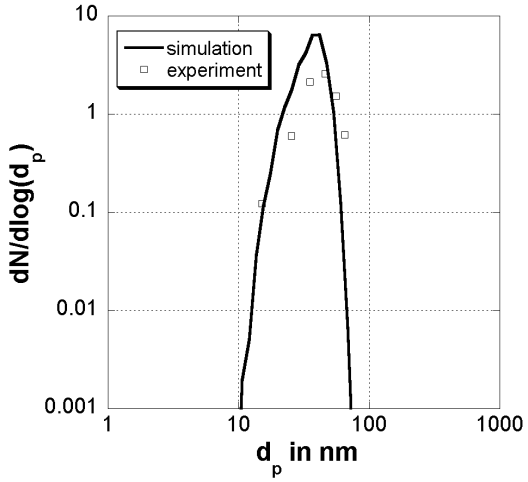

(c) 1750°C

Figure 11: *Primary particle size distribution for different final temperatures. The dots are experimental values from Seto et al [23].*

to the final temperature during 0.1s. The average collision diameter of the particles before reheating depends strongly on the time the particles are in the first reactor. The longer the particles are in the first reactor (where the particles are formed), the bigger is the collision diameter. In contrast the primary particle diameter does not depend so strongly on the time in the first reactor, only on the temperature.

Figure 11 shows the primary particle size distribution of the particles before reheating after 0.25s at 900°C, after reheating to 1500°C and after reheating to 1750°C. The temperature profile is the same as in the previous simulations. The distribution has been normalized to the total number of primary particles and divided by $\Delta \log(d_p)$. The dots are experimental values from Seto et al [23]. The primary particle size distribution before heating is quite narrow and no particle is bigger than 20nm. The primary particle size increases at higher temperatures and the distribution gets broader. The corresponding

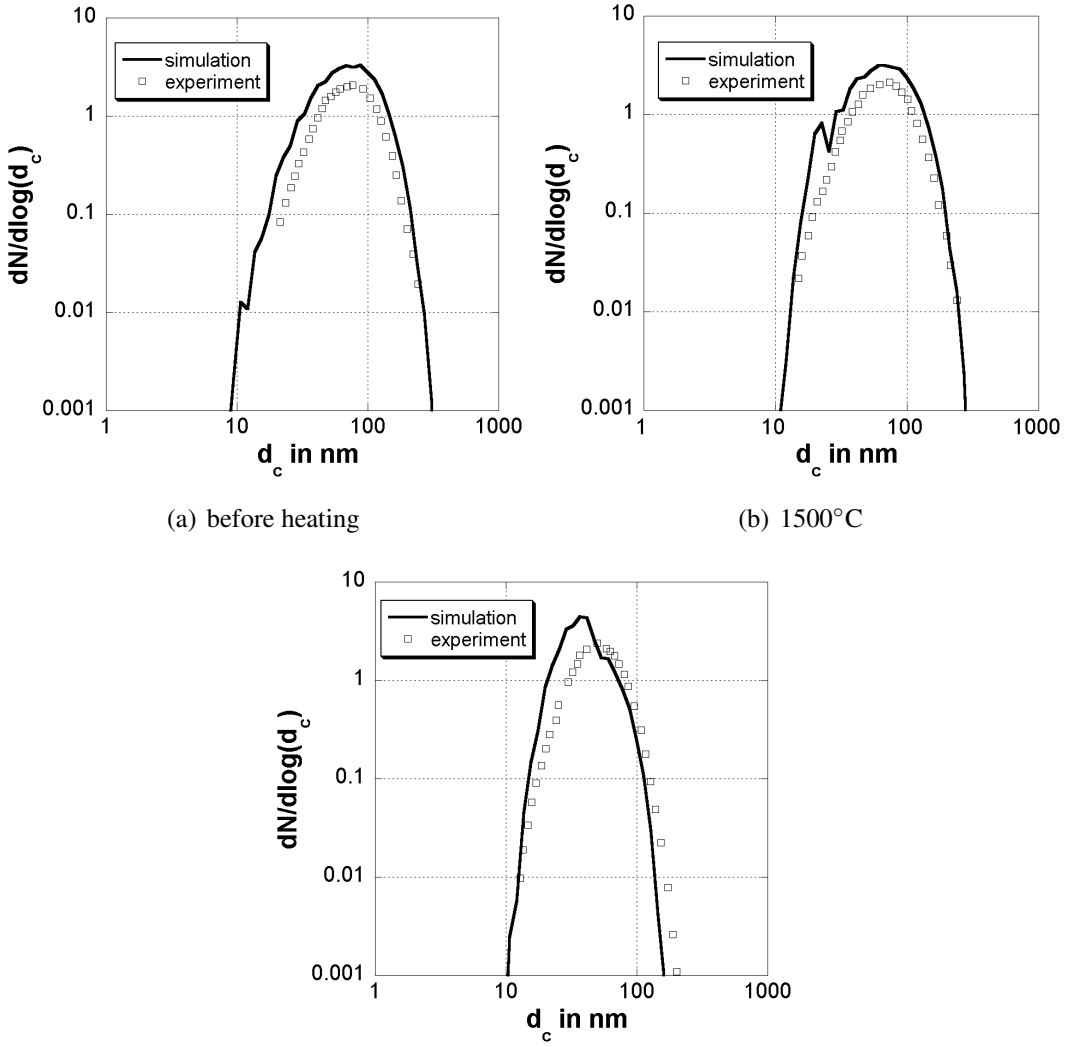

(a) before heating

(b) 1500°C

(c) 1750°C

Figure 12: *Collision diameter size distribution for different final temperatures. The dots are experimental values from Seto et al [23].*

collision diameter distributions are presented in Figure 12. The experimental values from Seto et al. [23] are the mobility diameter of the particles. In the comparison it is assumed that the mobility diameter is equal to the collision diameter. The collision diameter distribution gets narrower with an increasing temperature due to the sintering of the particles.
The average primary particle diameter for different final temperatures is shown in Figure 13. The dots are again experimental values from Seto et al. [23]. The particles do not sinter significantly before reaching 1500°C. After 1500°C the primary particle size increases strongly with increasing temperature. The particles are nearly spherical at 1850°C and most of the particles consist of only one primary particle, therefore further sintering processes are not possible. The primary particle diameter is equal to the collision diameter.
The particle structure does not depend on the collision diameter of the particles before

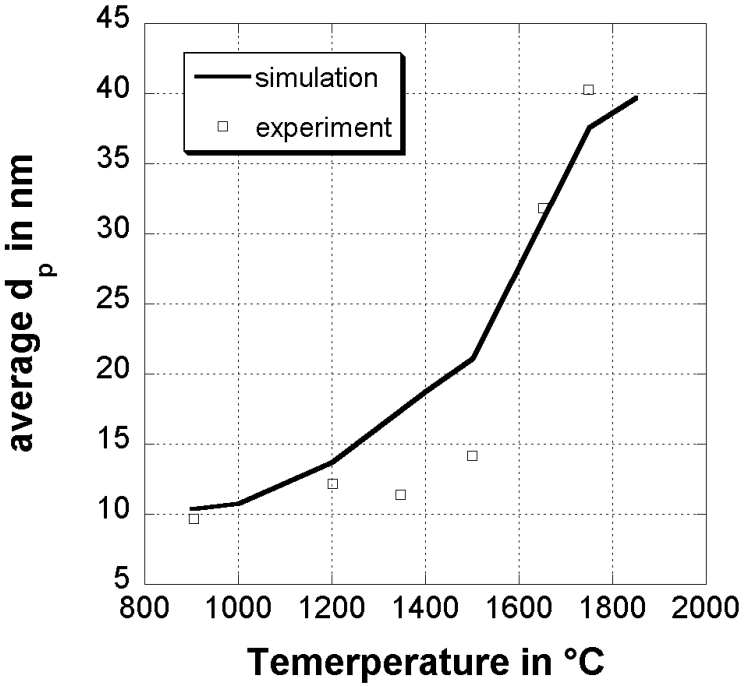

Figure 13: *Average primary particle diameter for different final temperatures. The dots are experimental values from Seto et al [23].*

heating. Figure 14 illustrates the average primary particle and collision diameters found for different times at which the temperature is increased (and hence for different collision diameters because particles held for a longer time at 900°C have bigger collision diameters). The particles have a collision diameter of 69nm and 83nm nm for a formation time of 0.2s respectively 0.3s. It is demonstrated that neither the primary particle diameter nor the collision diameter after the reheating depend on the particle size before reheating. Also the primary particle size distribution (see Figure 15) does not depend on the size of agglomerates before heating. Only the final temperature determines the shape of the particles. This is important if experimental values, where the residence time in the furnace is not clear, are compared to theoretical values. Computer generated TEM style images are compared to experimental values from Seto et al. [23] in Figure 16. The theoretical pictures have been created by colliding the primary particles that belong to each particle randomly. These particles have been shot at a plane to simulate the collection of particles using a TEM grid in an experiment. It is demonstrated that the particles shrink with increasing temperature and get rounder. The particles are nearly spherical at 1750°C.

5 Discussion

The sintering parameters A, E and $d_{p,min}$, presented in Table 1, depend on the material and are determined by fitting the model to the experimental data set. The parameters presented by Tsantilis [27] have been used as a starting guess. The difference in the parameters presented here and those used by Tsantilis arises from the different sintering

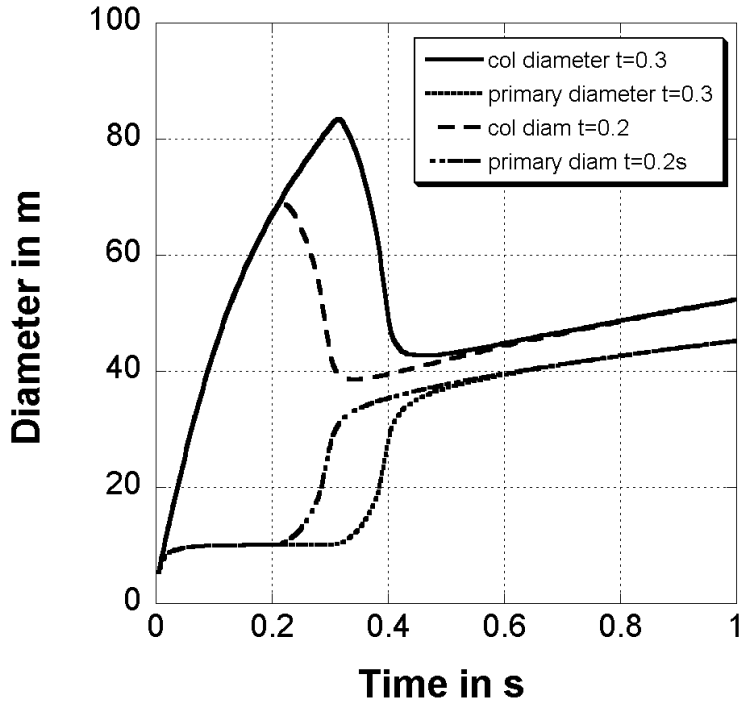

Figure 14: *Average primary particle and collision diameter for different times t_h where the temperature has been increased from 900°C to 1750°C during 0.1 s.*

models.
The sintering process starts already at temperatures that are lower then the melting point of the material, however even at temperatures higher than the melting point the particles are not completely spherical. It is also demonstrated that the primary particle diameter after reheating does not depend on the size of the particle before reheating. Also the residence time of the particles at the final temperature does not have an important influence on the shape of the particle. The particles reach their final shape shortly after the temperature has been increased. The primary particle diameter size distribution depends mainly on the highest temperature consequently the exact temperature profile is unimportant.
A sintering level (equation 8) has been defined to include the mass transfer between neighboring particles in the calculation of the characteristic sintering time. This is an empirical definition, however it is able to match experimental data. The sintering time without the mass transfer between the primary particles would be unrealistic low. In a further study we will try to get a more physical expression for the sintering level and the mass transfer between the particles using stochastic Monte Carlo algorithms similar to the method presented by Akhtar et al. [1].
The characteristic sintering time is calculated assuming that it is determined by the smaller primary particle [30]. This assumption has been fortified by simulating the system using the average primary particle diameter of the two neighboring particles as diameter. In this case the sintering time for small primaries connected to large primaries is very long and the final particles contain much more small primaries which is not consistent with experimental results.
The model enhances the previous primary particle list model [28] where sintering has

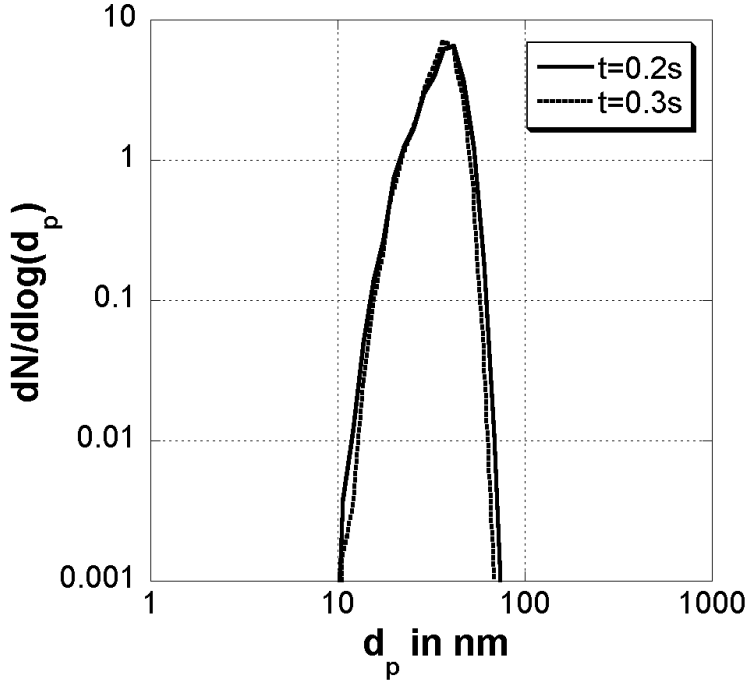

Figure 15: *Primary particle size distribution for different creation times t_h where the temperature has been increased from 900°C to 1750°C during 0.1 s.*

been calculated as an average for the entire particle. This is especially an issue when the primary particle size is broad because sintering of small primaries is underestimated. A comparison of the two models has demonstrated that the primary particle list model is not able to match the experimental observations for the formation of SiO_2 nanoparticles (the data obtained from the primary particle list model is not presented in this study).
The particle size and the primary particle size distributions are calculated from the first coagulation of two molecules and we make no assumption about the size distribution of the first particles. It is only determined by the coagulation of molecules from the gas-phase, whereas most sectional models assume a uniform primary particle size distribution at the beginning of the simulation.
In the current work gas-phase chemistry is not included due to the lack of existing thermochemistry and reaction rates for the formation of SiO_2. However the model is able to solve full gas-phase chemistry and in a further study a chemical mechanism for the formation of SiO_2 from TEOS will be developed using quantum chemical methods like density functional theory.
The computational performance of the model has been increased by using a binary tree data structure to store the particles and the primary particles. A typical simulation with 16384 stochastic particles takes about 3 hours of CPU time on one core of a 3 GHz Intel Harpertown cluster.

6 Conclusion

A stochastic particle model including unequal-sized primary particles has been presented and validated against experimental data. This model includes coagulation, condensation, inception and sintering. Each particle is described by the number of primary particles, the sintering level between neighboring primary particles and the volume of each primary particle. No assumption about the initial particle size distribution is made. The sintering is not calculated as an average but individually for each pair of neighboring particles. This is important if the primary particle size distribution is broad because the characteristic sintering time depends strongly on the size of the primaries. The underprediction of the sintering rate of small primary particles is avoided. The particles have been stored in a binary tree data structure to enhance the computational performance. The model is able match experimental data for the formation of SiO_2 nanoparticles in a hot wall reactor. The computer generated TEM images are comparable to experimental observations. The model is quite general and applicable to different materials by changing the sintering parameters.

Acknowledgements

Financial support from the EPSRC Grant No. EP/E01724X/1 and EP/C547241/1 is gratefully acknowledged. The authors thank Dr Murray Height from HeiQ Materials for financial and scientific support.

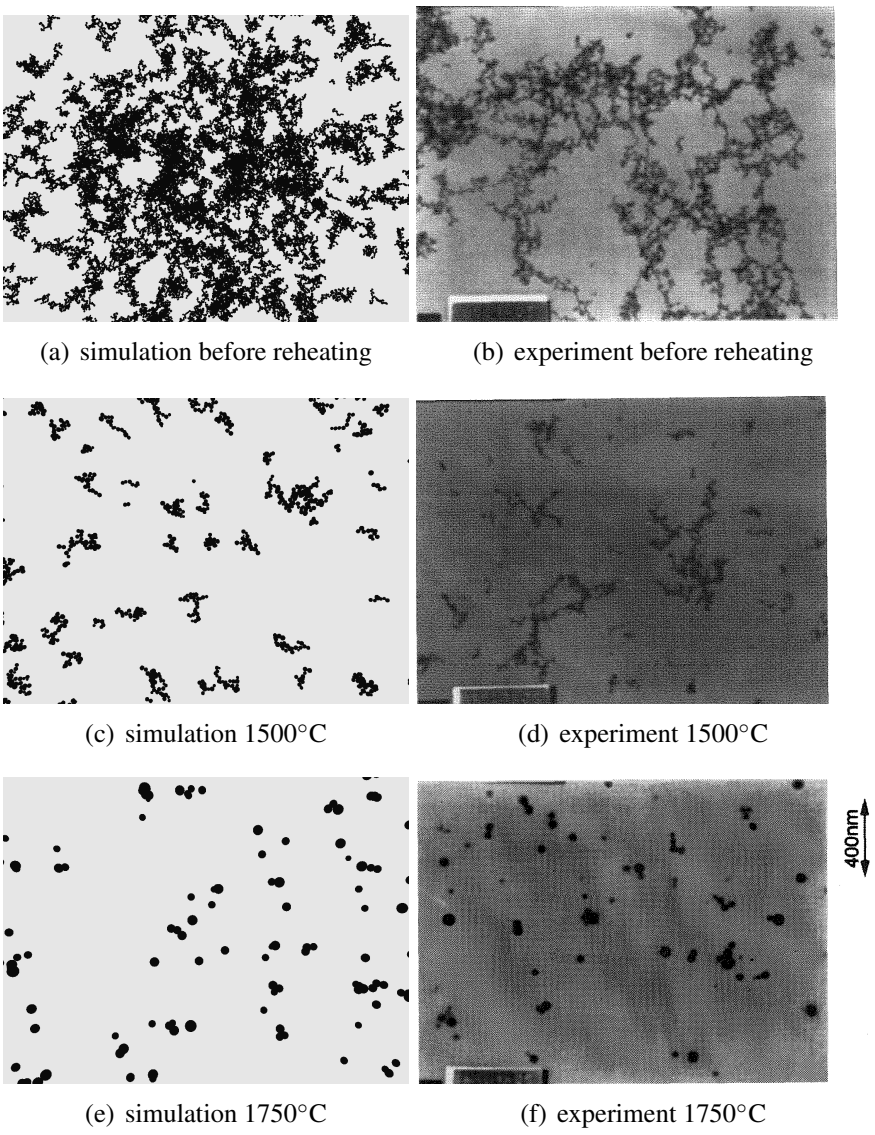

(a) simulation before reheating (b) experiment before reheating

(c) simulation 1500°C (d) experiment 1500°C

(e) simulation 1750°C (f) experiment 1750°C

Figure 16: *TEM style images at different final temperatures compared against experimental pictures from Seto et al [23]*

References

[1] M. K. Akhtar, G. G. Lipscomb, and S. E. Pratsinis. Monte carlo simulation of particle coagulation and sintering. *Aerosol Sci. Tech.*, (21):83–93, 1994. doi:10.1080/02786829408959698.

[2] M. S. Celnik, R. I. A. Patterson, M. Kraft, and W. Wagner. Coupling a stochastic soot population balance to gas-phase chemistry using operator splitting. *Combust. Flame*, 148(3):158–176, 2007. doi:10.1016/j.combustflame.2006.10.007.

[3] M. S. Celnik, M. Sander, A. Raj, R. H. West, and M. Kraft. Modelling soot formation in a premixed flame using an aromatic-site soot model and an improved oxidation rate. *Proc. Combust. Inst.*, (32):639–646, 2009. doi:10.1016/j.proci.2008.06.062.

[4] A. Eibeck and W. Wagner. Stochastic particle approximation for Smoluchowski's coagulation equation. *Ann. Appl. Probab.*, 11(4):1137–1165, 2001. doi:doi:10.1214/aoap/1015345398.

[5] A. Eibeck and W. Wagner. Stochastic interacting particle systems and nonlinear kinetic equations. *Ann. Appl. Probab.*, 13(3):845–889, 2003. doi:10.1214/aoap/1060202829.

[6] J. Frenkel. Viscous flow of crystalline bodies under the action of surface tension. *J. Phys.*, (9):385–391, 1945.

[7] M. Heine and S. E. Pratsinis. Polydispersity of primary particles in agglomerates made by coagulation and sintering. *J. Aerosol Sci.*, (38):17–38, 2007. doi:doi:10.1016/j.jaerosci.2006.09.005.

[8] W. Koch and S. K. Friedlander. The effect of particle coalesecence on the surface area of coagulating aerosol. *J. Colloid Interface Sci.*, (140):419–427, 1990. doi:10.1016/0021-9797(90)90362-R.

[9] N. Morgan, C. Wells, M. Kraft, and W. Wagner. Modelling nanoparticle dynamics: Coagulation, sintering, particle inception and surface growth. *Combust. Theor. Model.*, 9(3):449–461, 2005. doi:10.1080/13647830500277183.

[10] N. Morgan, M. Kraft, M. Balthasar, D. Wong, M. Frenklach, and P. Mitchell. Numerical simulations of soot aggregation in premixed laminar flames. *Proc. Combust. Inst.*, 31:693–700, 2007. doi:10.1016/j.proci.2006.08.021.

[11] H. Mühlenweg, A. Gutsch, A. Schild, and S. E. Pratsinis. Process simulation of gas-to-particle-synthesis via population balances: Investigation of three models. *Chem. Eng. Sci.*, (57):2305–2322, 2002. doi:10.1016/S0009-2509(02)00119-7.

[12] K. Nakaso, T. Fujimoto, T. Seto, M. Shimada, K. Okuyama, and M. M. Lunden. Size distribution change of titania nano-particle agglomerates generated by gas phase reaction, agglomeration, and sintering. *Aerosol Sci. Tech.*, (35):929–947, 2001.

[13] R. I. A. Patterson and M. Kraft. Models for the aggregate structure of soot particles. *Combust. Flame*, 151:160–172, 2007. doi:10.1016/j.combustflame.2007.04.012.

[14] R. I. A. Patterson, J. Singh, M. Balthasar, M. Kraft, and J. Norris. The Linear Process Deferment Algorithm: A new technique for solving population balance equations. *SIAM J. Sci. Comput.*, (28):303–320, 2006. doi:10.1137/040618953.

[15] R. I. A. Patterson, J. Singh, M. Balthasar, M. Kraft, and W. Wagner. Extending stochastic soot simulation to higher pressures. *Combust. Flame*, 145(3):638–642, 2006. doi:10.1016/j.combustflame.2006.02.005.

[16] A. Raj, M. Celnik, R. Shirley, M. Sander, R. Patterson, R. West, and M. Kraft. A statistical approach to develop a detailed soot growth model using pah characteristics. *Combust. Flame*, (Accpeted for publication). doi:10.1016/j.combustflame.2009.01.005.

[17] S. N. Rogak. Modeling small cluster deposition on the primary particles of aerosol agglomerates. *Aerosol Sci. Tech.*, (26):127–140, 1997. doi:10.1080/02786829708965419.

[18] M. Sander, A. Raj, O. Inderwildi, M. Kraft, S. Kureti, and H. Bockhorn. The simultaneous reduction of nitric oxide and soot in emissions from diesel engines. *Carbon*, (47):866–875, 2009. doi:10.1016/j.carbon.2008.11.043.

[19] D. W. Schaefer and A. J. Hurd. Growth and structure of combustion aerosols: fumed silica. *Aerosol Sci. Tech.*, 12:876–890, 1990. doi:10.1080/02786829008959400.

[20] H. Schmid, B. Al-Zaitone, C. Artelt, and W. Peukert. Evolution of the fractal dimension for simultaneous coagulation and sintering. *Chem. Eng. Sci.*, (61):293–305, 2006. doi:10.1016/j.ces.2004.11.068.

[21] H.-J. Schmid, S. Tejwani, C. Artelt, and W. Peukert. Monte carlo simulation of aggregate morphology for simultaneous coagulation and sintering. *J. Nanoparticle Res*, (6):613–626, 2004. doi:10.1007/s11051-004-2161-x.

[22] T. Seto, M. Shimada, and K. Okuyama. Evaluation of sintering of nanometer-sized titania using aerosol method. *Aerosol Sci. Tech.*, (23):183–200, 1995. doi:10.1080/02786829508965303.

[23] T. Seto, A. Hirota, T. Fujimoto, M. Shimada, and K. Okuyama. Sintering of polydisperse nanometer-sized agglomerates. *Aerosol Sci. Tech.*, (27):422–438, 1997. doi:10.1080/02786829708965482.

[24] J. Singh, M. Balthasar, M. Kraft, and W. Wagner. Stochastic modelling of soot particle size and age distribution in laminar premixed flames. *Proc. Combust. Inst.*, 30:1457–1465, 2005.

[25] J. Singh, R. I. A. Patterson, M. Kraft, and H. Wang. Numerical simulation and sensitivity analysis of detailed soot particle size distribution in laminar premixed ethylene flames. *Combust. Flame*, 145:117–127, 2006. doi:10.1016/j.combustflame.2005.11.003.

[26] S. Tsantilis and S. E. Pratsinis. Evolution of primary and aggregate particle-size distributions by coagulation and sintering. *AIChE*, (46):407–415, 2000. doi:10.1002/aic.690460218.

[27] S. Tsantilis, H. Briesen, and S. E. Pratsinis. Sintering time for silica particle growth. *Aerosol Sci. Tech.*, (34):237–246, 2001.

[28] R. H. West, M. S. Celnik, O. R. Inderwildi, M. Kraft, G. J. O. Beran, and W. H. Green. Towards a comprehensive model of the synthesis of TiO_2 particles from $TiCl_4$. *Ind. Eng. Chem. Res.*, 46(19):6147–6156, 2007. doi:10.1021/ie0706414.

[29] Y. Xiong and S. E. Pratsinis. Formation of agglomerate particles by coagulation and sinterings – part I. a two-dimensional solution of the population balance equation. *J. Aerosol Sci.*, 24:283, 1993. doi:10.1016/0021-8502(93)90003-R.

[30] V. Yadha and J. Helble. Modeling the coalescence of heterogenous amporphous particles. *J. Aerosol Sci.*, (35):665–681, 2004. doi:10.1016/j.jaerosci.2003.11.009.